SEISMIC RETROFITTING OF A 14-STOREY Y-SHAPE HOSPITAL IN NORTHERN ITALY

I.G. Colombo[1], L. Radice[2], P. Martinelli[3] & M. di Prisco[4]

[1,2] DSC Erba Srl, Erba (CO), Italy

[3] Department of Civil and Environmental Engineering, Politecnico di Milano, Milan, Italy

[4] DSC Erba Srl, Erba (CO), Italy - Department of Civil and Environmental Engineering, Politecnico di Milano, Milan, Italy - marco.diprisco@dscerba.com

Abstract: *An in-depth analysis of the seismic vulnerability of an existing hospital located in the North of Italy revealed pounding issues among the seven blocks that constitute the 14-storey reinforced concrete (RC) building, standing 50 meters tall and buit in the 1960s. The contraction joints, designed for thermal and shrinkage deformations, are characterized by a very limited opening (30 mm). The building has an irregular Y-shape and a bearing structure consisting of RC beam-column frames, with cast-in-place concrete walls of various shapes and positions serving as shear-resistant elements. The structure underwent an extensive diagnostic campaign to characterize materials and verify the correspondence of reinforcement with the original structural design project. Additionally, dynamic tests were carried out using micro-seismic acquisition to determine the structure's free vibration frequencies and vibration modes. These tests revealed only partially active joints. The vulnerability assessment, encompassing the definition of the actual behaviour of the structure at Serviceability and Ultimate Limit States, was performed through finite element linear dynamic and push-over analyses, both developed using commercial software. Based on the results, a retrofitting proposal was designed, which involves the closure of the roof joints at the top of the building and the retrofitting of some critical columns and several walls for shear resistance. Closing the joints only at the roof floor addresses pounding problems, minimizing the impact of the intervention on the hospital's operability and the number of unverified elements. A connecting C45/55 concrete plate measuring 3.0×2.0×0.2 m^3 is assumed, placed in the attic across the joint and connected to the underlying brick-cement floor using post-tensioned Ø30 threaded vertical bars. The adjacent brick lightening will be removed and filled with poured concrete. The concrete plate will be transversely post-tensioned using threaded rods. The shear retrofitting of staircases is analysed, considering the possible introduction of suitably designed active mass dampers.*

1. Introduction

Assessing the seismic vulnerability of critical infrastructure in the building stock, especially strategic facilities like hospitals and those dedicated to civil protection, is crucial to ensure operational continuity even during extreme conditions. A significant portion of strategic buildings, including those accommodating large crowds like schools, was initially designed without sufficient seismic considerations. Examining the Italian building stock, various studies underscore the significant vulnerability of strategic and school buildings when exposed to seismic forces (Perrone et al., 2015; Ruggieri et al., 2021). In the context of hospital buildings, particularly those located in seismically demanding areas, existing structures often struggle to meet essential safety requirements. The literature offers a wide range of strengthening systems for reinforced concrete (RC) frame structures. Limiting our attention to the retrofitting of RC existing hospitals, notable works propose various solutions. For instance, Syrmakezis et al. (2006) proposed two strengthening methods: (i) concrete jackets around column and beam elements, and (ii) the application of viscoelastic dampers to enhance structural stability. Xu et al. (2022) suggested a novel external sub-structure for retrofitting old school-hospital RC frame structures in near-fault regions. This external sub-structure comprises precast bolt-connected steel-plate reinforced concrete buckling-restrained-brace-frame. In a separate study, Mazza (2021) proposed the strengthening of a five-storey RC framed structure with exterior and interior in-plan distributions of hysteretic damped braces. Pisapia et al. (2023) provided two main solutions to improve the structural performance of an existing hospital made of RC cores connected to a steel structure. The first approach involves augmenting the thickness of the existing RC cores, while the second solution entails reinforcing the RC cores through the application of steel plates, steel strips, and angles.

A prevalent characteristic in strategic buildings, such as hospitals, is the existence of expansion joints with narrow widths, typically ranging from 30 to 50 mm, that separate two or more independent blocks. These joints were primarily designed to accommodate temperature and shrinkage strains. However, as many of these buildings were originally designed to withstand gravity and wind loads only, the limited width of the joints poses challenges for meeting current seismic standards, especially concerning pounding verifications. Consequently, modern earthquake-resistant design codes necessitate a minimum seismic gap between adjacent buildings or within structures divided into two or more independent units. Construction details must facilitate two-dimensional relative out-of-phase movements between these blocks.

The paper investigates the seismic vulnerability and proposes a retrofitting strategy for a 14-storey RC building comprising distinct independent blocks. The case study pertains to a strategic structure situated in Northern Italy, initially designed solely for gravity and wind loads. Consequently, the building's seismic performance is deemed inadequate, and its classification as a 'strategic building' raises concerns about very high seismic risk. Additionally, ensuring uninterrupted functionality during the retrofitting process is a crucial objective.

2. Building description

The building, designed in 1963-'64, comprises 14 floors, including a basement floor (S2), a semi-basement floor (S1), a mezzanine floor (R), and eleven above-ground floors (P1 to P10 + S). With a Y-shaped plan (see Figure 1), the structure is divided into seven blocks, extending from floor S2 to floor S, with expansion joints providing separation between the blocks. Notably, for the lower five floors, the building is interconnected with an adjacent building, as highlighted in Figure 1. The structural drawings illustrate nominal structural joints, each measuring 30 mm in width. These joints are present between the various blocks of the building and specifically between block C and the adjacent buildings. The reduced size of these joints is justified by their intended purpose of accommodating thermal expansion in the materials. Importantly, these joints were not originally designed to account for displacements resulting from seismic forces.

Continuous foundations were constructed for all blocks. Foundation beams run parallel to the longitudinal direction of the blocks at the axes of the columns and are interconnected through transverse beams. In areas where elevator shafts and plant cavities are situated, direct plate foundations are connected to the foundation beams.

Concrete floors consist of slabs pre-assembled on site with a width of 120 cm, including three rows of hollow clay blocks each. These slabs are constructed continuously over three bays, have a maximum net span of 4.75 m, and a height of 23 cm (20+3). Blocks A, B, F, and G are characterized by a hollow clay block floor with a height of 28+2 cm. In the case of block C, the hollow clay block floors used are of the cast-in-place, with a height of 24+3 cm; these are constructed continuously over two bays, with a maximum span of 7.40 m for the reference floor.

The elevation structure comprises cast-in-place concrete columns and beams. The columns, primarily rectangular, are reinforced with longitudinal bars ranging from 12 to 32 mm in diameter, along with Ø6/20 stirrups. Some columns have irregular shapes, accommodating angles in the building plan. Longitudinally running downstand beams, continuous over several bays, have a maximum span of 6.50 m. In areas where the "Verona" floor is adopted, the floor direction is inverted. RC cores function as braces for the structures. Their layout in the plan is not based on structural criteria for a homogeneous distribution of stiffness, but rather depends on distributive-architectural aspects. Figure 2 illustrates the structural plan of the typical floor (P1 to P9) of E block, highlighting bracing cores in green, beams in orange, and expansion joints in grey.

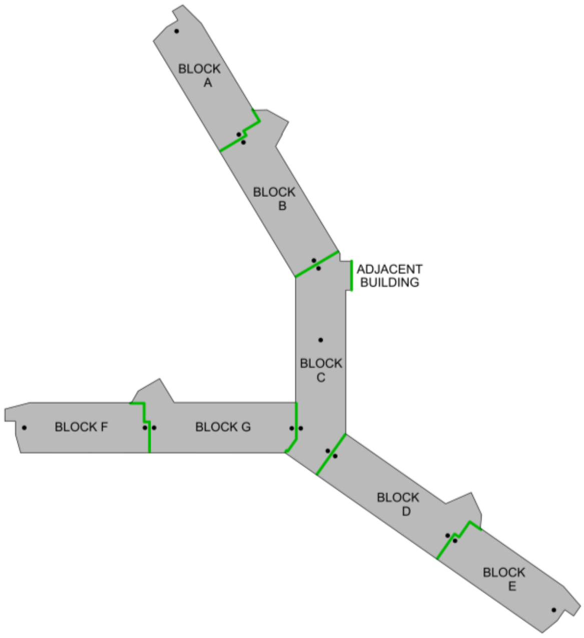

Figure 1. Plan view of the building, showing expansion joints in green, independent blocks, maximum dimensions, and accelerometer location (black dots).

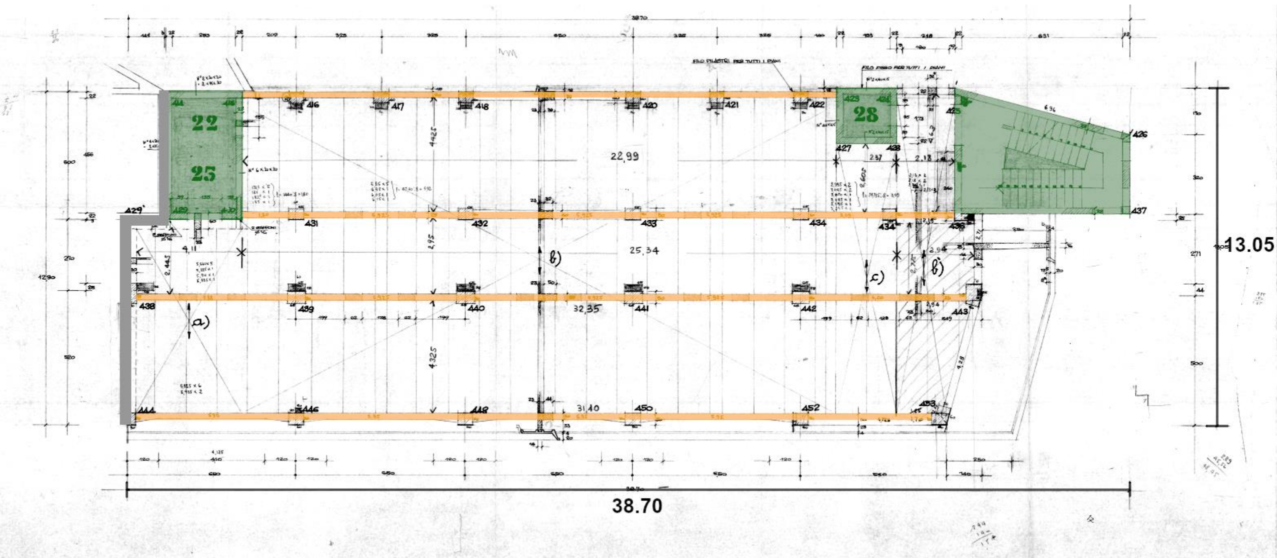

Figure 2. Structural plan (floor P1 to P9) of block E: in green stairwells-lift cores, in orange beams, and in grey expansion joints.

3. Survey campaign

3.1 Experimental investigation on materials

The structural drawings specified a concrete mix with 300 kg/m³ of cement (R730), with the provision for 400 kg/m³ in highly stressed elements. Concrete strength is determined according to 'Servizio Tecnico Centrale del Consiglio Superiore dei Lavori Pubblici della Repubblica Italiana' (2017), considering the mean value of the cubic compressive strength of n specimens ($R_{cm(n)is}$) reduced by the confidence factor (FC). An intermediate knowledge level (LC2) with FC = 1.20 is assumed. A total of 51 cores were extracted from walls and columns, with 47 related to concrete with 300 kg/m³ of cement. Based on the results, cylindrical design values for compressive strength (17.03 MPa and 19.38 MPa) were used for ductile mechanism verifications. Corresponding values, reduced by the material safety coefficient of 1.5, are employed for brittle mechanism checks.

Aq50 steel was prescribed for column and wall reinforcement, while FeB44k steel with $\sigma_s \geq 431$ MPa was specified for floors and beams. Aq50 has a nominal yield strength above 270 MPa and a nominal ultimate tensile strength of 500-600 MPa. According to Verderame et al. (2011), the average yield strength is assumed 370.9 MPa (mean value calculated over 3278 specimens with SD of 31.84 MPa). Durometer tests at 45 + 6 locations for both steel classes align with the types specified at the design stage.

3.2 Ambient vibration tests of the building

Micro-seismic accelerometers were employed for dynamic tests, capturing minimal oscillations from seismic background noise or wind thrust. The positions and orientations of accelerometers are illustrated in Figure 3a. These tests facilitated the determination of natural frequencies and vibration mode shapes. Figure 3b presents a sketch of the first mode shape identified experimentally. Table 3 reports the first four experimental natural frequencies, with noteworthy similarity in the frequencies of the first three modes, despite being associated with different branches of the building. The table also specifies the vibration mode types. Additional tests, placing accelerometers along the height of the extreme staircases in the three branches of the building, confirmed the absence of inflection points for the first eight modes.

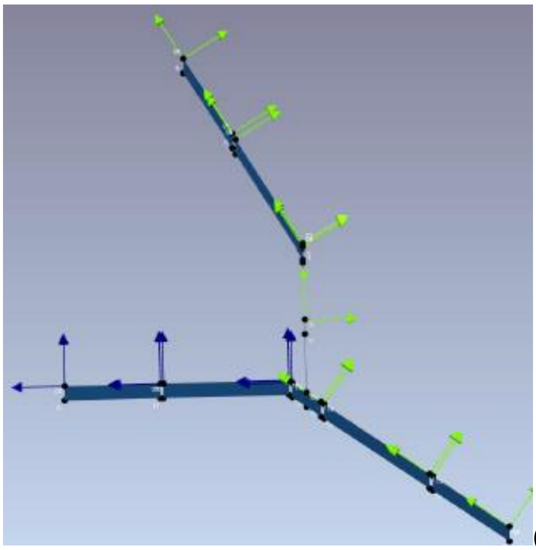
(a)

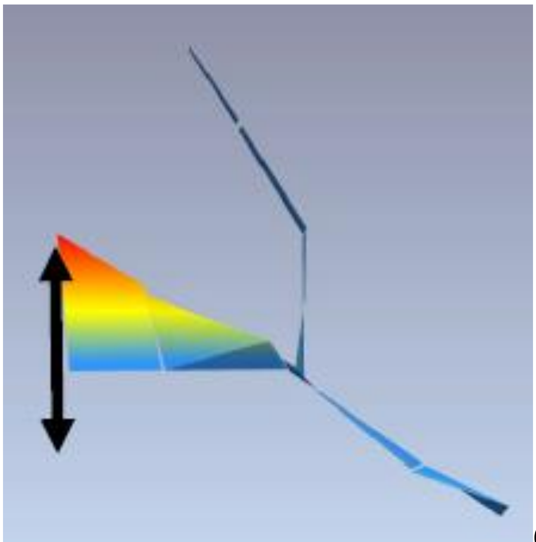
(b)

Figure 3. (a) simplified geometrical model with position and direction of accelerometers (b) first modal deformation experimentally detected (Courtesy of 4 EMME Service S.p.A.).

Table 1. Experimental natural frequencies, periods and modes type.

Mode No.	Frequency (cycle/sec)	Period (sec)	Type
1	1.03	0.97	Transversal translation of F-G blocks (with a pivot on block C)
2	1.08	0.93	Transversal translation of D-E blocks (with a pivot on block C)
3	1.10	0.91	Transversal translation of A-B blocks (with a pivot on block C)
4	1.29	0.76	Transversal translation of C block

4. Structural modelling

To assess vibration modes, displacements, and internal forces/moments on structural elements, finite element (FE) structural models are made using Midas Gen software (2022). One-dimensional beam elements represent columns and beams, while two-dimensional 'wall' type elements are chosen for elevator shaft and stairwell RC walls, and plate elements for retaining walls. Figure 4 displays a 3D view of the FE structural model of the building. For seismic analysis, infinite stiffness is assumed in the plane of the floors (horizontal diaphragm). Seven separate diaphragms, one for each block, are considered for each plane. Fixed-end conditions are assumed at the base of walls and columns, with out-of-plane displacements prevented for retaining walls. Structural permanent load is calculated based on slab type, while non-structural permanent load considers weights of screeds, pavements, and vertical partitions. Live load is determined from technical drawings.

The seismic action on the building is represented through a response spectrum, influenced by site seismic hazard and soil type, aligning with the Italian Building Code (NTC 2018, 2018) and Eurocode 8 principles (CEN, 2004). Assuming a nominal life $V_N = 50$ years and a coefficient of usage $C_u = 2$, the reference period $V_R = C_u \times V_N$ results in 100 years. With a soil type of class C and a topographic amplification factor of 1.0, the building, irregular in both plan and elevation, experiences a horizontal peak ground acceleration (PGA) of 0.059 g for the Life Safety Limit State (LSLS). A behaviour factor q = 1.5 is considered. Response spectrum analyses (RSA) focus solely on the horizontal components of seismic motion, involving 32 load combinations derived from four positions of the centre of mass associated with eight possible combinations of seismic action components in both horizontal directions.

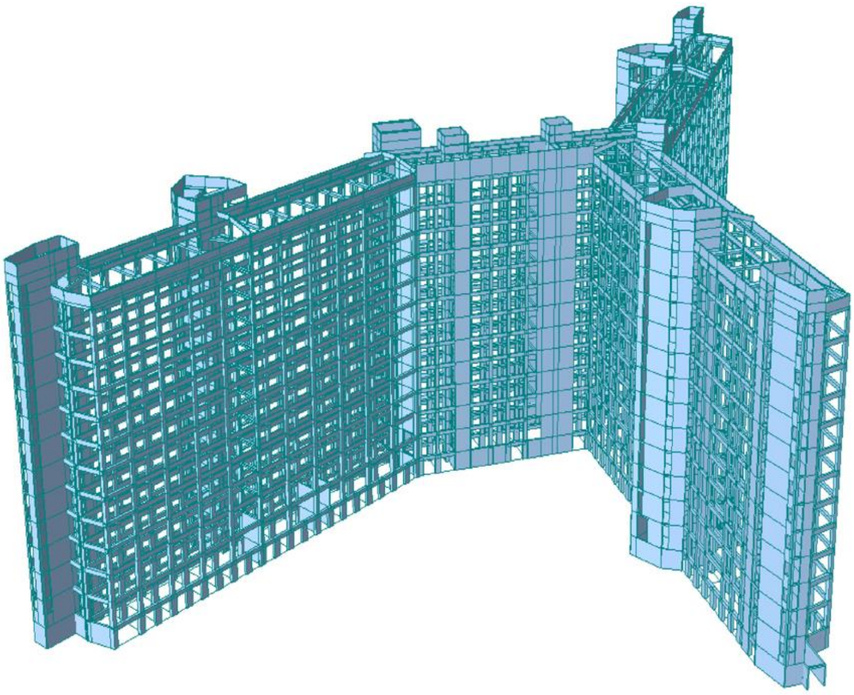

Figure 4. FE model of the building.

Table 2 displays the first vibration modes of each building block, identified through modal analysis, along with the corresponding percentage of participating mass for each mode. Notably, the initial mode associated with block C is the 12th, reflecting its elevated stiffness due to a greater number of RC walls in that section of the building. Figure 5 provides visual representations of the deformations linked to three specific numerical modes of vibration: modes 1, 2, and 12.

The experimental findings indicate that, although structural joints exist among the seven constituent blocks of the building, these joints exhibit partial activity. The dynamic test outcomes reveal that the blocks do not operate independently; instead, the displacement of each block appears influenced by adjacent block displacements. Consequently, a direct comparison of modal deformations between experimental and numerical results is challenging. Regarding main mode frequencies, numerical values range from 0.51 Hz to 1.28 Hz (considering modes 1 to 21 with significant mass activation), while experimental values range from 1.03 Hz to 2.45 Hz. Despite utilizing fixed-end constraints and assuming non-cracked concrete in the finite element model, it exhibits less rigidity than the experimental data. This discrepancy can be attributed to several factors: (i) neglecting the stiffening contribution of unmodeled infill walls; (ii) introducing live loads with values potentially higher than those during experimental measurements; (iii) the simplified modelling of joints, assumed perfectly active in the numerical model, but only partially in reality; and (iv) the absence of constraints at connections with adjacent buildings.

To replicate the first experimental frequency more accurately, an additional numerical model was generated by deactivating all relative motions at the expansion joints and constraining displacement in alignment with the adjacent building. This updated finite element model yields a first natural frequency of 0.90 Hz (compared to the prior value of 0.51 Hz). Further enhancements in frequency could be achieved by incorporating the modelling of infill walls and minimizing the impact of acting accidental loads.

Table 2 – Numerical modes of vibration

Mode No. (block)	Frequency (cycle/sec)	Period (sec)	TRAN-X MASS (%)	SUM (%)	TRAN-Y MASS (%)	SUM (%)	ROTN-Z MASS (%)	SUM (%)
1 (D)	0.5092	1.964	1.2812	1.2812	6.8782	6.8782	3.3757	3.3757
2 (E)	0.519	1.9268	3.8295	5.1106	4.2755	11.1537	18.7521	22.1279
3 (F)	0.5241	1.9081	0.2134	5.3241	7.747	18.9008	9.732	31.8599
4 (B)	0.5244	1.9069	7.1455	12.4696	0.7892	19.6899	4.1515	36.0114
5 (G)	0.537	1.8621	0.2164	12.686	8.565	28.2549	0.9694	36.9808
6 (A)	0.6624	1.5097	5.0802	17.7663	2.2328	30.4876	14.3561	51.3369
12 (C)	0.8351	1.1975	12.9931	57.0852	0.0743	43.8705	0.0154	54.6286

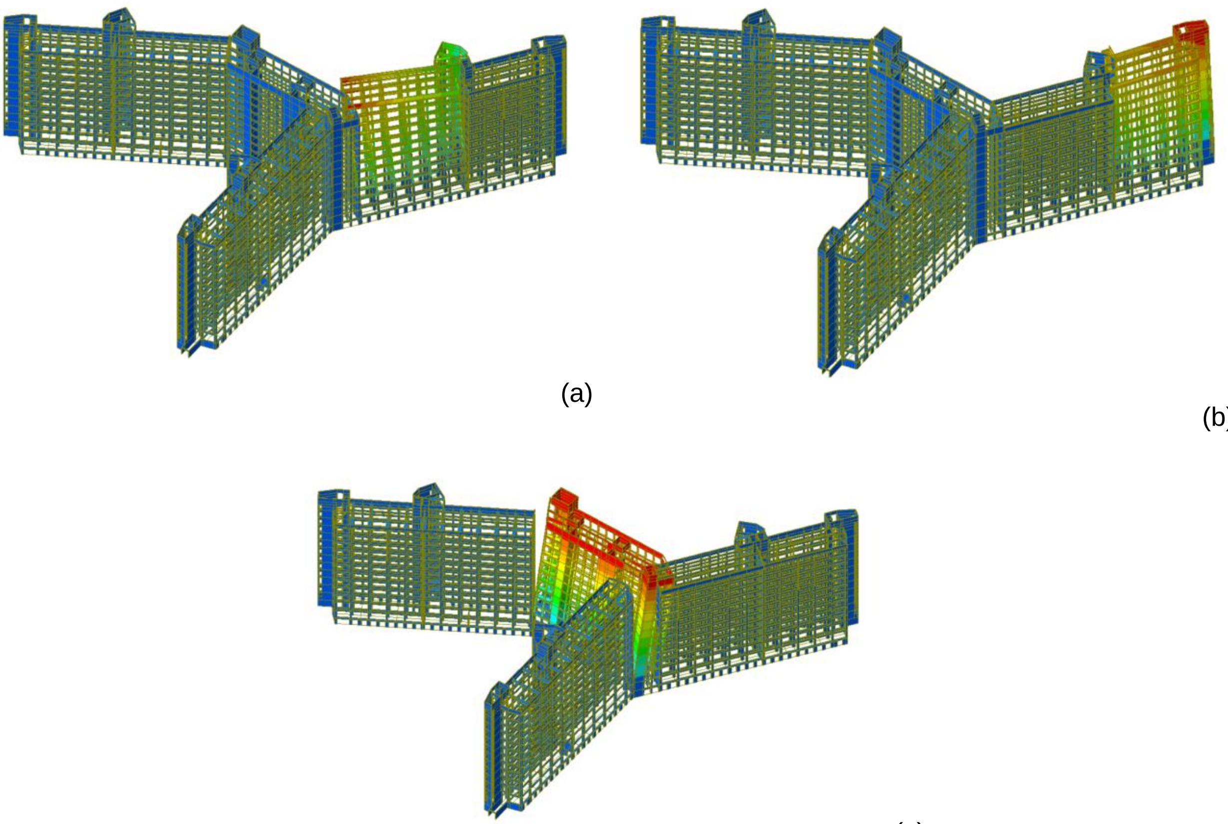

(a) (b) (c)

Figure 5. (a) First, (b) second, and (c) twelfth numerical mode shapes before strengthening interventions.

5. Seismic vulnerability assessment of the existing building

To examine the potential seismic interaction between blocks arising from restricted joint openings, horizontal displacements of points near these joints are computed, considering the LSLS (NTC 2018, 2018):

$$d_E = \mu_d d_{Ee} \tag{1}$$

$$\mu_d = q \qquad \text{if } T_1 \geq T_c \tag{2}$$

$$\mu_d = 1 + (q-1)\frac{T_c}{T_1} \quad \text{if } T_1 < T_c \quad \text{(in any case } \mu_d \leq 5q-4\text{)} \tag{3}$$

In eq. (1) d_{Ee} represents the horizontal displacement obtained from the linear dynamic analysis. As an example, the values of d_{Ee} for points placed on F-G and G-C joints are collected in Table 3.

Table 3 –Horizontal displacement d_{Ee} at LSLS obtained from the FE analysis. (F_G means the displacement of block F towards G)

	Joint F_G		**Joint G_F**		**Joint G_C**		**Joint C_G**	
	$d_{Ee,x}$ (mm)	**$d_{Ee,y}$ (mm)**	**$d_{Ee,x}$ (mm)**	**$d_{Ee,y}$ (mm)**	**$d_{Ee,x}$ (mm)**	**$d_{Ee,y}$ (mm)**	**$d_{Ee,x}$ (mm)**	**$d_{Ee,y}$ (mm)**
S	31.42	50.69	42.67	31.21	42.67	84.96	40.93	26.39

The greatest maximum relative displacement occurs between block G and block C in the local y-direction (indicated by blue cells in the table), reaching an amplified value of 167 mm when multiplied by 1.5. However, across all joints, the relative displacement at the top storey (S) exceeds the nominal joint width of 30 mm in both the x and y directions. This indicates a pounding issue between the building's constituent blocks, resulting in a Safety Index for pounding problems of 18%.

Moreover, considering bending and shear with this model, unattended verifications revealed a Safety Index of 19% in bending and 29% in shear. Consequently, based on verifications for pounding, bending, and shear, assuming perfectly active joints and elastic non-cracked behaviour, an overall Safety Index of 18% could be assigned to the building, corresponding to the minimum of the three values mentioned above.

6. Closure of the roof joints

To address the pounding issue and mitigate the forces exerted on the vertical elements, the analysis considers connecting the blocks at three points for each structural joint, specifically at the upper floor of the building (floor P10 - storey S). This intervention aims to enable the building to behave as a single block, minimizing significant relative displacements between the slabs of unconnected floors.

In the FE model, the connection of the blocks involves the punctual insertion of translational springs that link the end nodes of the columns and walls. The stiffness assigned to these springs is uniform in both directions and assumes a delamination length of 4 bar diameters, with a specific value:

$$k = \frac{EA}{4\phi} = \frac{190000 \cdot 14130}{120} = 2.24 \cdot 10^7 \, \frac{\text{N}}{\text{mm}} \tag{4}$$

The design of the connections relies on the maximum force experienced by the translational springs. Specifically, at each connection point, 64+64Ø30 post-tensioned 10.9 steel bars, embedded in concrete blocks (class C45/55) affixed to the structure, are incorporated. Each concrete block measures 3.0×2.0×0.2 m³ and is transversally post-tensioned through 21Ø30 10.9 steel bars, tightened with a bolt torque of 393 kN. Along the joint, there are the edge beams of the floor and the lightweight “Bisap” type brick-cement floor, running parallel to these beams. The adjacent brick lightening will be removed, and concrete will be poured in their place. The effective tangential and normal stiffness of this solution is larger than that incorporated in the FE model.

Table 4 presents the outcomes of the modal analysis for the strengthened building, indicating the percentage of participating mass associated with each individual vibration mode. Figure 6 illustrates the deformed shape of the first three vibration modes.

Table 4 – Post-strengthening first three numerical vibration modes

Mode No	Frequency (cycle/sec)	Period (sec)	TRAN-X MASS (%)	SUM (%)	TRAN-Y MASS (%)	SUM (%)	ROTN-Z MASS (%)	SUM (%)
1	0.6585	1.5187	7.9992	7.9992	2.0993	2.0993	56.7999	56.7999
2	0.742	1.3477	43.0969	51.0961	20.4969	22.5963	2.0823	58.8822
3	0.8359	1.1963	15.8849	66.981	45.1369	67.7331	7.2303	66.1125

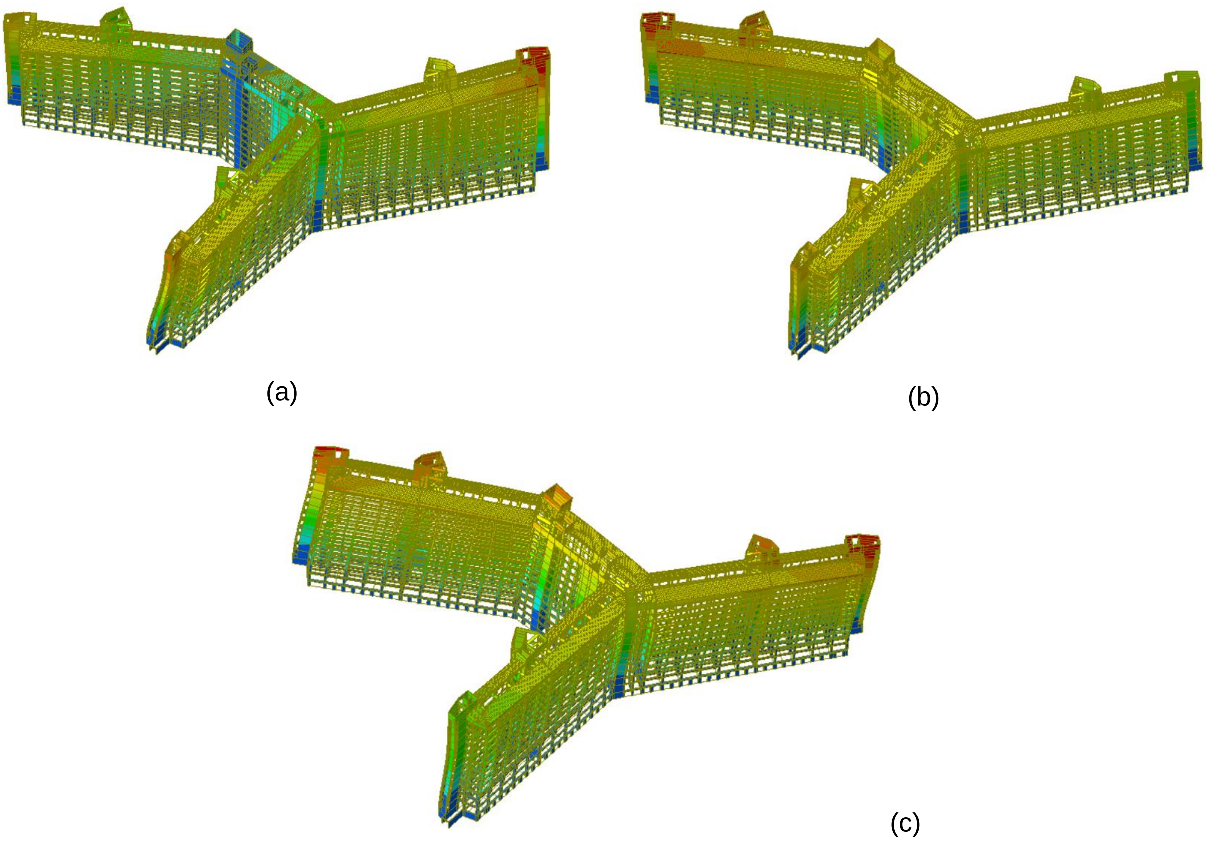

(a) (b) (c)

Figure 6. (a) first, (b) second, and (c) third numerical mode shapes after strengthening interventions.

The reassessment of pounding, previously conducted for the building composed of distinct blocks, is reiterated for the unified structure. It is noteworthy that, in extrapolating displacements from the model, those associated with the first three modes, characterized by the same sign (lacking inflection points along the deformation), are excluded. By summing the absolute values of displacements in these modes, the threshold of 30 mm is not reached. Thus, it is confirmed that these displacements do not give rise to pounding issues between unconnected blocks on the floors. This cautious approach ensures safety, as even for higher modes, displacements sometimes share the same sign and do not accumulate as absolute values.

The assessment focuses on floor P4, where the most significant displacements are observed among the floors with unclosed joints. Specifically, the greatest relative displacement occurs at the joint between block F and block G, with a maximum displacement ($d_{E,max}$) of 12.27 mm (computed with $\mu_d = 1.5$). Consequently, the intervention effectively resolves issues related to seismic pounding between adjacent blocks.

7. Seismic vulnerability assessment after the closure of the joints

As already specified in Section 5, the building, in its current form, is characterized by a bending Safety Index of 19%. Even after closing the joints at the top of the building, flexural weakness persists when the structure is analysed through a linear dynamic analysis. To account for the non-linear resources of the structure, such as structural redistribution, a non-linear static analysis (pushover) was conducted. This analysis employed a displacement control approach, using either the centre of gravity of the distributed mass on the top floor or, alternatively, the point on the roof with the maximum displacement in the considered direction as the control point. As the first mode of vibration does not reach a mass participation of 75%, the distribution corresponding to the plane forces acting on each floor, calculated in the linear dynamic analysis, was used. This involved considering 50 modes with a total mass participation greater than 85%. Specifically, the following cases were considered: X+, e+; Y+, e+; X-, e-; Y-, e- (with X and Y representing forces in the X and Y directions, and "e" standing for eccentricity, while "+" and "-" indicate the orientation). Due to difficulties in numerical convergence, additional cases were not considered. A second group of distributions is foreseen by the national standard, as it provides a good description of the post-peak behaviour. However, due to numerical convergence issues, the pushover curves stop at displacement values close to the peak. Nevertheless, these values still allow the execution of the required checks, making the application of this second group of distributions considered unnecessary.

Plastic hinges, with properties defined according to the Italian Standard (NTC 2018, 2018), were incorporated at the base and top of RC columns and walls (resulting in 2 plastic hinges for each floor space of each element) and at the ends of the beams. Only bending plastic hinges were considered; shear plastic hinges were not introduced. Shear checks (for brittle mechanisms) refer to the results obtained from the linear dynamic analysis.

The M-ϑ constitutive law for plastic hinges is elastic-plastic. The behaviour remains linear up to the point of plasticization of the hinges (M-ϑ_y); after the formation of the hinges, the rotation increases, while maintaining a constant moment value. The yield rotations (ϑ_y) and ultimate rotations (ϑ_u) are defined as prescribed in the Circular of NTC 2018 (2019). The plasticization moment of the section corresponds to the rotation ϑ_y.

As required by Eurocode 8 – Part 3 (CEN 2005), a cracked flexural stiffness must be employed for the elements, with the value corresponding to the slope of the first branch of the moment-curvature law of the plastic hinges at the ends of the elements (over a length equal to L/6). For the extremities, an EI value equal to 0.2 times $EI_{uncracked}$ can be considered, as recommended by *fib* Bulletin 25 (2003). Given the necessity to assign a single stiffness value to the elements in resolving the frame, and lacking a precise evaluation of the stiffness properties, the decision was made to utilize cracked flexural and shear stiffness equal to half the uncracked elastic stiffness of the gross section (as suggested in point 9.4(3) of Eurocode 8– Part 1, CEN, 2004).

The pushover results, depicting base shear versus displacements, are illustrated in Figure 8. Upon comparing the demand and capacity for each Limit State as mandated by the standard, it is observed that global verifications for ductile mechanisms are met at both the Serviceability Limit States (SLO and SLD according to the Italian National Standards) and the Ultimate Limit States (SLV and SLC according to the same National Standards).

The state of the plastic hinges is assessed at the step corresponding to the Life Safety Limit State (demand). Specifically, the check ensures that the hinges do not reach the SD (Significant Damage) limit, which corresponds to a rotation equal to 0.75 ϑ_u. As illustrated in Figure 8, focusing on the most critical distribution in the X direction, the state of the plastic hinges is presented in terms of RY rotation. RY represents the rotation with the Y-axis as the unit vector in the local reference system of the individual element, where the Y-axis is oriented orthogonally to the plane of the wall. No reinforced concrete wall or column exceeds the limit set by the standard, indicating that no vertical element is critical from a flexural standpoint at LSLS. It is worth noting that the green hinges represent sections where the moment of plasticization has been reached, placing them on the plateau of the moment-rotation law of the plastic hinges.

The same check was carried out at the Limit State of Collapse, ensuring that the hinges do not reach the NC (Near Collapse) limit, which corresponds to a rotation equal to ϑ_u. Once again, no column or wall exceeds this limit, confirming that no vertical element is critical from a flexural standpoint. Regarding shear, being a brittle mechanism, the element check was developed by considering the results of the linear dynamic analysis performed at SLSL with the inelastic spectrum (behaviour factor q equal to 1.5). In Figure 9, columns and walls that have not been verified are highlighted in red (assuming a slope of the concrete strut equal to 45°).

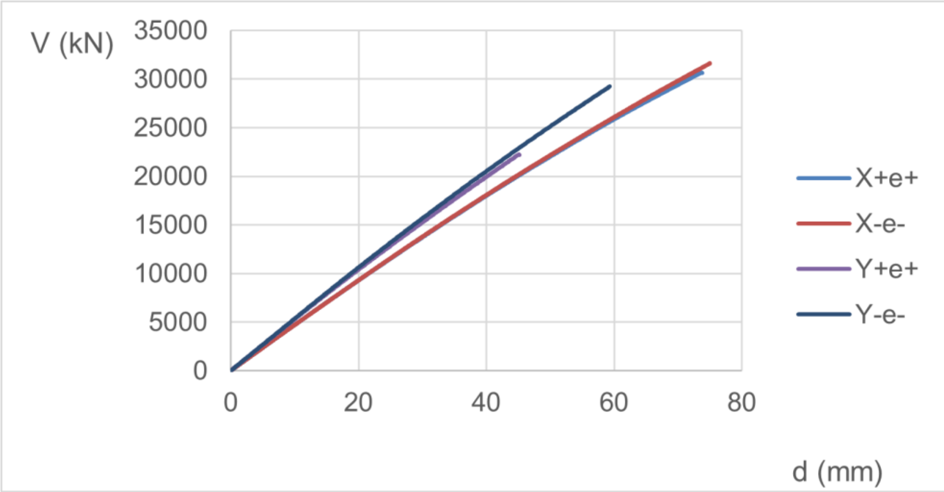

Figure 7. Base shear vs. displacement curves.

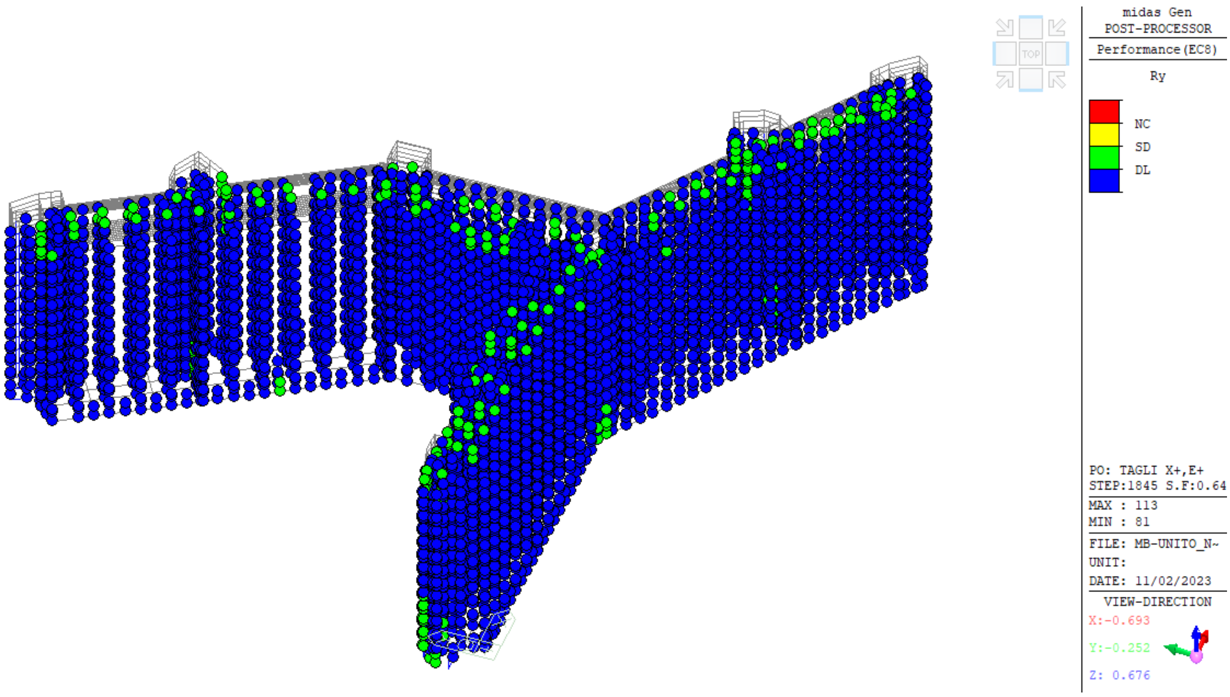

Figure 8. RY rotation in columns and walls at LSLS for the most critical distribution in X-direction.

From the automatic calculation of the FE software, 962 "Wall" elements in shear are identified as not verified. Considering the first cracking shear value, this number is reduced to 364,without considering the effect of axial force. For these walls, we propose the application of a retrofitting system consisting of a 15 mm thick Fibre Reinforced Cementitious Matrix (FRCM). The fabric should be unidirectional and applied horizontally on both sides of the wall, whenever possible. In cases where this is not feasible due to the presence of inter-storey slabs, steel plates fixed using pass-through connectors will be used to secure the system. The key characteristics of the system include a composite conventional limit strength of 2097 MPa (on concrete support) and an equivalent thickness of 0.091 mm.

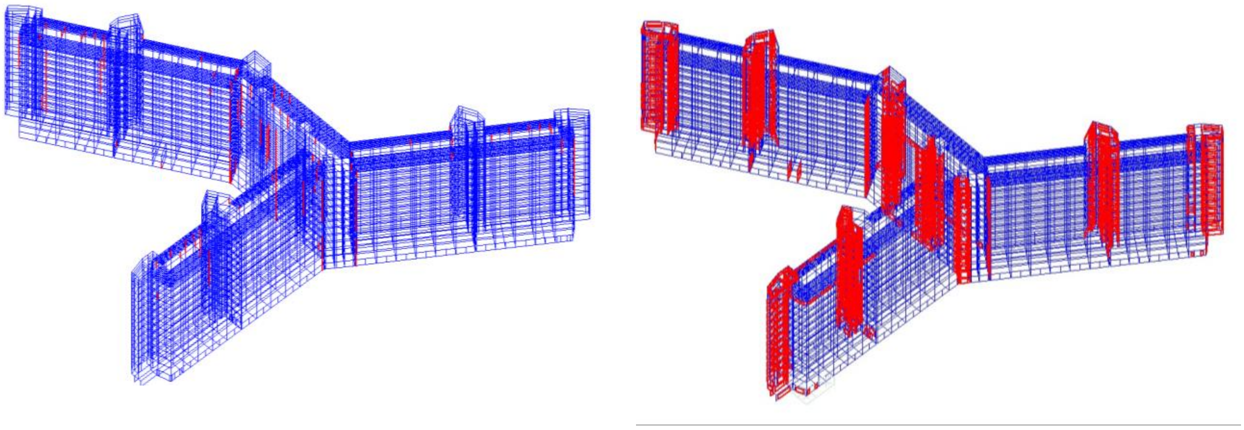

Figure 9. Columns and walls not verified in shear.

8. Active Mass Dampers

To assess the potential reduction of the retrofitting intervention on walls designed with the consideration of FRCM composite, a preliminary evaluation was carried out on the application of an innovative damping system. Consequently, the Active Mass Damper (AMD) technology was considered (Rebecchi et al. 2022). This active system is created using inertial masses controlled by an electro-mechanical actuator, generating forces that act directly on the building, typically on the roof or top floor where they are most effective.

A reasonable number of AMDs was assumed, specifically 5+5 AMDs modelled through nonlinear dashpots introduced at the closure of each roof joint (storey S), resulting in a total of 60 masses. It is challenging to envision the application of a larger number of AMDs, given that the considered storey is occupied by facilities.

A preliminary result of the study is presented in Figure 10, where the base shear in x direction versus time is plotted, revealing a 17% reduction in peak values. Considering y direction, the reduction is equal to 14%. For this preliminary evaluation, the LSLS elastic spectrum was considered to process the spectrum-compatible accelerograms, and only one accelerogram was used.

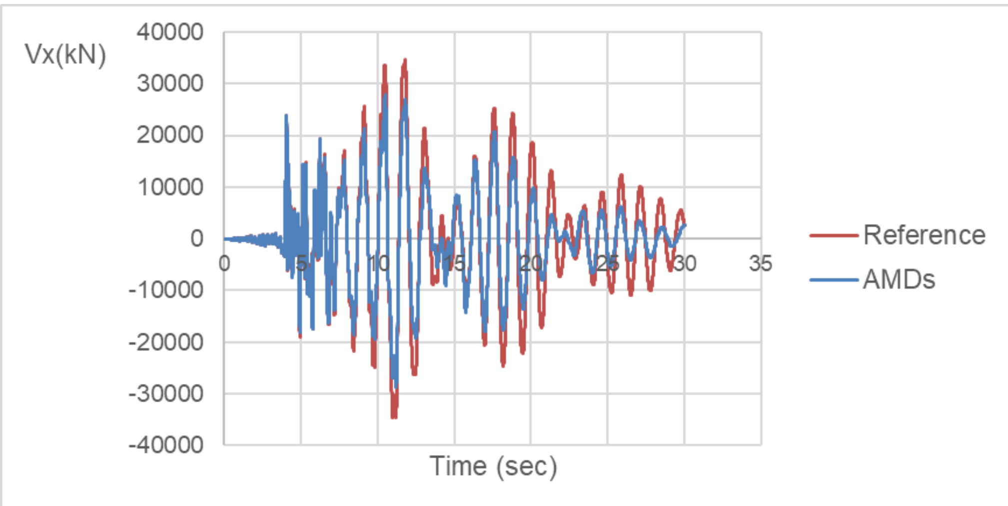

Figure 10. Base shear (in X direction) vs. time curve.

9. Conclusions

The paper addresses the seismic vulnerability of a high-rise reinforced concrete (RC) building comprising various independent blocks. It proposes a straightforward and cost-effective retrofitting strategy. The case study pertains to a hospital located in northern Italy originally designed for gravity and wind loads only. The issue arises from the limited width of the expansion joints, which fails to meet pounding verifications – a common concern in strategic buildings like hospitals. Combining ambient vibration tests with numerical simulations revealed that the expansion joints are only partially active. The retrofitting strategy primarily involves the incorporation of RC link systems on the upper floor. This approach has proven successful, not only enhancing earthquake resistance, and eliminating pounding effects (thereby reducing internal forces/moments on columns), but also allowing the building to remain functional during the seismic retrofitting intervention. To minimize the extent of the strengthening intervention by using FRCM, a preliminary study is conducted on the potential benefits of employing active mass dampers.

10. Acknowledgements

The support of 4 EMME Service S.p.A and Nuove Iniziative S.p.a. for the diagnostic and dynamic experimental investigation is gratefully acknowledged. Eng. Fabio Menardo (Head of Structural Engineering in ISAAC srl) and Dr. Giovanni Rebecchi (Technical Sales Manager in ISAAC srl) are gratefully acknowledged for their substantial help in the preliminary design of the Active Mass Damper system.

11. References

CEN (2004). EN 1998-1:2004. Eurocode 8: Design of structures for earthquake resistance — Part 1: General rules, seismic actions and rules for buildings. European Committee for Standardization (CEN), Brussels.

CEN (2005). EN 1998-3:2005. Eurocode 8: Design of structures for earthquake resistance — Part 3: Assessment and retrofitting of buildings, Comité Européen de Normalisation, Brussels.

fib Bulletin 25. (2003). Displacement-based seismic design of reinforced concrete buildings. Lausanne

Mazza, F. (2021). In-plane and out-of-plane nonlinear seismic response of masonry infills for hospitals retrofitted with hysteretic damped braces, *Soil Dynamics and Earthquake Engineering*, 148, 106803.

MIDAS Gen (2022). MIDAS Information Technology Co

MIT Ministero delle infrastrutture e dei trasporti Circolare 21 gennaio 2019, n. 7 (2019). Istruzioni per l'applicazione dell'Aggiornamento delle "Norme tecniche per le costruzioni", Gazz Uff Della Repubb Ital (In Italian)

NTC 2018 (2018). Aggiornamento delle norme tecniche per le costruzioni. Decreto del Ministro delle Infrastrutture del 17 gennaio 2018. Gazzetta Ufficiale Serie Generale n. 42 del 20-02-2018 (in Italian)

Perrone D., Aiello M.A., Pecce M., Rossi F. (2015). Rapid visual screening for seismic evaluation of RC hospital buildings, *Structures*, 3:57–70. https://doi.org/10.1016/j.istruc.2015.03.002

Pisapia, A., Piluso, V., Montuori, R., Nastri, E., Frattolillo, C. (2023). Seismic Assessment and Structural Retrofitting of the Day-Hospital Building "G. Pascale Foundation", *Appl. Sci*, 13(3), 1663.

Rebecchi G., Calvi P.M., Bussini A., Dacarro F., Bolognini D., Grottoli L., Rosti M., Ripamonti F., Cii S. (2022). Full-Scale Shake Table Tests of a Reinforced Concrete Building Equipped with a Novel Servo-Hydraulic Active Mass Damper, *Journal of Earthquake Engineering*, DOI: 10.1080/13632469.2022.2121338

Ruggieri S., Porco F., Uva G., Vamvatsikos D. (2021). Two frugal options to assess class fragility and seismic safety for low-rise reinforced concrete school buildings in Southern Italy, *Bull Earthq Eng*, 19(3):1415–39

Servizio Tecnico Centrale del Consiglio Superiore dei Lavori Pubblici della Repubblica Italiana. (2017). Linee Guida per la Valutazione delle Caratteristiche del Calcestruzzo in Opera. (In Italian).

Syrmakezis C.A., Mavrouli O.A., Antonopoulos A.K. (2006). Rehabilitation of hospital buildings using passive control systems, *Smart Struct Syst*, 2–4:305–312. https://doi.org/10.12989/sss.2006.2.4.305

Verderame G.M., Ricci P., Esposito M., Sansiviero F.C. (2011). Le caratteristiche meccaniche degli acciai impiegati nelle strutture in c.a. realizzate dal 1950 AL 1980 (in Italian). In: AICAP

Xu J.G., Cao, X.Y., Gang W. (2023). Seismic collapse and reparability performance of reinforced concrete frames retrofitted with external PBSPC BRBF sub-frame in near-fault regions, *J. Building Eng*, 64, 105716. https://doi.org/10.1016/j.jobe.2022.105716